Dynamic Gait Monitoring Mobile Platform

Robin Amsters[1,4], Ali Bin Junaid[1,4], Nick Damen[1], Jeroen Van De Laer[1], Benjamin Filtjens[1,2,3,4], Bart Vanrumste[2,3] and Peter Slaets[1,4]

[1]*Department of Mechanical Engineering, KU Leuven, 3000 Leuven, Belgium*

[2]*Department of Electrical Engineering (ESAT), STADIUS - IMEC, KU Leuven, 3001 Heverlee, Belgium*

[3]*eMedia Research Lab, KU Leuven, 3000 Leuven, Belgium*

[4]*Intelligent Mobile Platform Research Group, KU Leuven, 3000 Leuven, Belgium*

Keywords: Gait Analysis, Kinect, Mobile Robot, Kalman Filter.

Abstract: Human gait is an important indicator of health. Existing gait analysis systems are either expensive, intrusive, or require structured environments such as a clinic or a laboratory. In this research, a low-cost, non-obtrusive, dynamic gait monitoring platform is presented. By utilizing a mobile robot equipped with a Kinect sensor, comprehensive gait information can be extracted. The mobile platform tracks the skeletal joint movements while following the person. The acquired skeletal joint data is filtered to improve detection. Gait parameters such as step length, cadence and gait cycle time are extracted by processing the filtered data. The proposed approach was validated by using a VICON motion capture system. Results show that the proposed system is able to accurately detect gait parameters but requires a calibration procedure. Even though the camera is moving while tracking, the performance is on par with existing works. Step times can be detected with an average accuracy of around 10 milliseconds. Step length can be detected with an average accuracy of a few centimeters.

1 INTRODUCTION

An aging society is widely considered to be one of the main socio-political challenges of the 21st century. Demographic studies conclude that the European population is aging rapidly (European Commission, 2014). The share of those aged 80 years or above is projected to more than double between 2015 and 2080 (from 5.3% to 12.3%). Due to the decreasing number of nursing professionals, the lack of available assisted living facilities and the growing number of people who require regular monitoring, there is a serious imbalance in providing satisfactory healthcare services (Liu and Liu, 2014). Automated healthcare systems are, therefore, in high demand and there is growing attention for technologies that support elderly people. Robotic systems are an example of such technologies. They can assist in the rehabilitation and care of patients or elderly in their own home. Researchers aim to develop systems which can autonomously monitor health indicators with minimal human intervention.

One of the most important indicators of health decline is human gait. The use of gait data covers a wide range such as treatment of diabetes (Hodgins, 2008) and neurological diseases (Keijsers et al., 2006; Hausdorff et al., 2000). It can also be used to detect other adverse events such as decline of physical functions and fall incidents (Hausdorff et al., 2001; Van Kan et al., 2009; Viccaro et al., 2011; Peel et al., 2013). Non-intrusive and precise gait measurement systems can be applied in diagnosis, health monitoring, treatment and rehabilitation (Hodgins, 2008; Wren et al., 2011), assisting in early diagnosis and assessment (Keijsers et al., 2006; Hoff et al., 2001) and measuring medication effectiveness at home (Keijsers et al., 2003) without the need for patients to reside in rehabilitation or nursing homes.

Researchers have proposed several methods for gait analysis. The most popular tool to study gait is based on motion capture systems which use IR cameras and markers placed on the subject (Mihradi et al., 2011a; Mihradi et al., 2011b). Despite being accurate and precise, these systems are often very expensive and require complex setup by placing markers on the subject's body before each recording. This makes them suitable only for laboratory settings. Force plates are also used for gait analysis, which are also

Amsters, R., Bin Junaid, A., Damen, N., Van de Laer, J., Filtjens, B., Vanrumste, B. and Slaets, P.
Dynamic Gait Monitoring Mobile Platform.
DOI: 10.5220/0006733200490061
In *Proceedings of the 4th International Conference on Information and Communication Technologies for Ageing Well and e-Health (ICT4AWE 2018)*, pages 49-61
ISBN: 978-989-758-299-8

very costly and thus only applicable in labs and clinics. Furthermore, continuous analysis is not possible due to a fixed sensor setup and a limited measurement range or field of view.

Recent studies proposed the use of wearable sensors (Yang and Hsu, 2010; O'Donovan et al., 2009). Such systems are more suitable for ambulatory measurements in mobile settings as they are small, lightweight and less expensive. Insole pressure sensors are also used to measure gait parameters (Crea et al., 2014). However, wearable sensors have some drawbacks as well. Gravity, noise and signal drift must be taken into account (Luinge and Veltink, 2005). Sensors must also be placed correctly before analysis (Kavanagh and Menz, 2008). Markerless optical gait detection systems have been discussed in the context of biometric identification and surveillance. Single or multiple video cameras can be used to recognize individuals (Goffredo et al., 2010). Another markerless technique was proposed in (Yoo and Nixon, 2011) but the accuracy of extracted stride parameters was not verified. Leu et al. (Leu et al., 2011) focused on extraction of knee joint angles, but not on standard stride requiring complex setup and calibration. Van Den Broeck et al. proposed a monitoring system based on audio senors (Van Den Broeck et al., 2013). Small and relatively low-cost microphone arrays were used to estimate the location of footsteps. A best median of errors of 31cm was achieved, but this accuracy depends on the relative position of the microphones and the feet.

In this research, a non-intrusive, low-cost system that can accurately measure a wide range of gait parameters is proposed which offers a solution for the aforementioned problems. The system utilizes a mobile robot equipped with a Kinect depth camera. This is an array of sensors, including a stereo camera and a depth sensor, enabling it to extract a 3D virtual skeleton of the body (Shotton et al., 2013). Being an affordable choice, several researchers have already proposed the usage of a Kinect for monitoring and gait analysis (Stone and Skubic, 2011a; Stone and Skubic, 2011b; Baldewijns et al., 2014). The combination with a mobile platform enables continuous monitoring by following a person and capturing the movement and trajectory of the subject. The field of view is concentrated on the person itself and is less disturbed by influences such as other people or moving objects. With our proposed active subject tracking system, limitations of the fixed test space and camera occlusions are minimized. Post-processing of the acquired data allows us to evaluate the gait ability in terms of cadence, step length and gait cycle time. The proposed study presents a method for mobile monitoring of gait parameters which can be applied in many environments. The only requirement is that the floor should be relatively even (as is the case in most indoor space without stairs). This will allow the subject to perform their regular daily activities while the robot simultaneously tracks the movement and extracts gait parameters.

2 METHODOLOGY

The proposed solution enables dynamic gait monitoring by following a person and tracking it's joint positions. The robot starts by finding a person in the environment. Presence of a person is detected via images from the webcam on a laptop. A detection algorithm was written based on the open source image processing library OpenCV [1]. More specifically, the Haar feature-based cascade classifier that is proposed in (Viola and Jones, 2001) was used. This is a machine learning based approach that trains a cascade function from images. Alternatively, one could use the images from the kinect instead of the webcam. However, the webcam was much easier to interface with OpenCV. The OpenNI package that tracks the joint positions occupies the kinect USB port and does not provide access to the images. Accessing these images with other programs would require significant modifications to the OpenNI source code. Seeing as a laptop was already present on the platform for user interaction (see section 3.1), we opted to use the onboard laptop for presence detection. The kinect is solely used to track the joints.

If a person is detected for the first time, a sound is played to indicate that the user should perform a 'psi pose' (see Figure 1). When the psi pose is successfully detected, another sound is played. This tells the user that they can turn around and start walking. The robot then initializes the skeleton tracking and starts following the person while maintaining a fixed distance from the person. The joint coordinates are saved and gait data is extracted in post-processing (see section 2.3). In case the target is not in the field of view of the camera, the robot starts looking for the target again. If the person is then found again, tracking resumes. Figure 2 shows the aforementioned control scheme.

2.1 Following the Subject

The mobile platform serves as a tool to track and monitor the person simultaneously. Figure 3 illustrates the process.

[1] http://opencv.org/

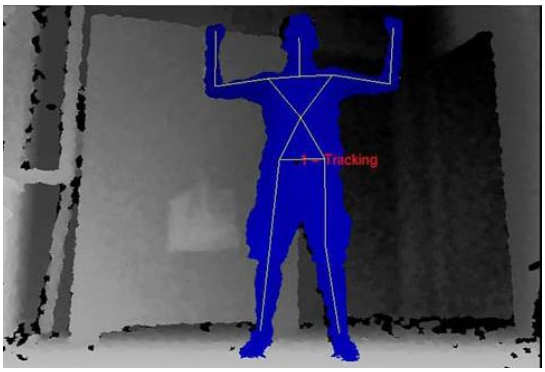

Figure 1: Initializing the tracking of a person by performing the ”psi pose”.

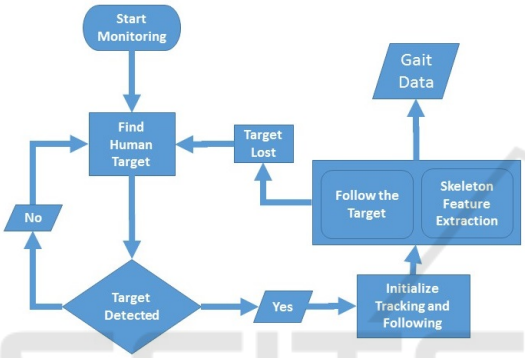

Figure 2: Control Scheme.

The Kinect provides depth measurements of the subject. To keep the person in the middle of the image frame, a controller was implemented. This enables better detection of the joints. The goal of this controller is to keep a constant distance of 1.3m between the person and the robot. This distance provides a good view for a person of average height. Additionally, the robot should drive in the same direction as the person is walking. Both the distance and the angle can be controlled by applying either a linear or a rotational velocity to the robot. The linear velocity is controlled with a state feedback controller. This type of controller places the poles of the closed loop system at a pre-determined place in the imaginary plane (Sontag, 2013). Figure 4 shows the feedback loop of the controller.

This control scheme relies on the formulation of a state-space model. The model can be obtained by applying a step input to the motors of the robot, and identifying the parameters from the subsequent response. This leads to the following state space model:

$$\boldsymbol{A} = \begin{bmatrix} 0 & 1 \\ -0.2 & -0.5 \end{bmatrix} \quad \boldsymbol{B} = \begin{bmatrix} 0 \\ 2 \end{bmatrix} \quad \boldsymbol{C} = \begin{bmatrix} 1 & 0 \end{bmatrix} \quad (1)$$

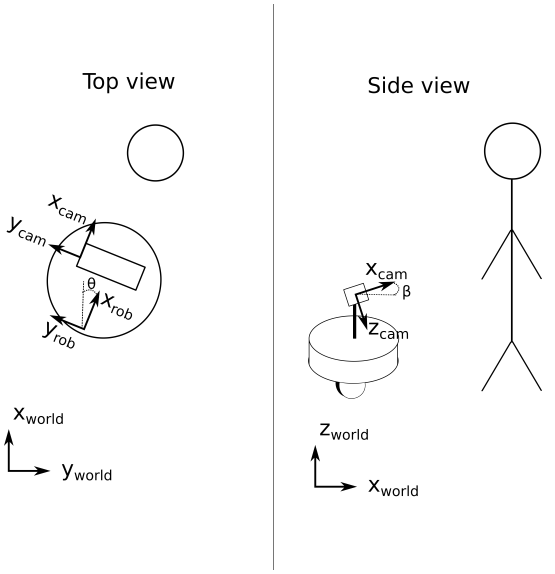

Figure 3: Human tracking with the mobile robot. Left: top view of the system. Right: side view of the system.

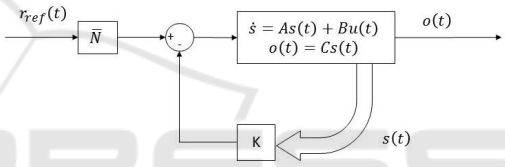

Figure 4: State feedback controller (Wahid et al., 2010). The state vector consists of the robot speed and acceleration along the x-axis ($[\boldsymbol{s}] = [\dot{x}, \ddot{x}]$), the reference r_{ref} is the desired distance between the robot and the person, the output o is the translational speed of the robot. $\boldsymbol{K}$ and $\boldsymbol{N}$ are the feedback and feedforward matrices, respectively.

The closed loop poles are defined by the desired controller response. The feedback matrix $\boldsymbol{K}$ can then be determined via pole placement. A feedforward gain matrix $\boldsymbol{N}$ is added to control the state around a constant value other than 0. This leads to the following controller parameters:

$$\boldsymbol{K} = \begin{bmatrix} 22.2057 & 4.75 \end{bmatrix} \quad \boldsymbol{N} = \begin{bmatrix} 2.2239 \end{bmatrix} \quad (2)$$

These parameters provide satisfactory steady state behavior. However, in case the robot is starting from a stationary position, then the response is too fast. Test subjects did not have enough time to comfortably start walking from a standstill. Therefore we also determined a feedback and feedforward gain matrix that provide a slower response. These parameters are only used at the start of the experiment.

$$\boldsymbol{K} = \begin{bmatrix} 0.8064 & 0.75 \end{bmatrix} \quad \boldsymbol{N} = \begin{bmatrix} 0.4888 \end{bmatrix} \quad (3)$$

Besides keeping an appropriate distance, the heading angle of the robot should also be aligned with the

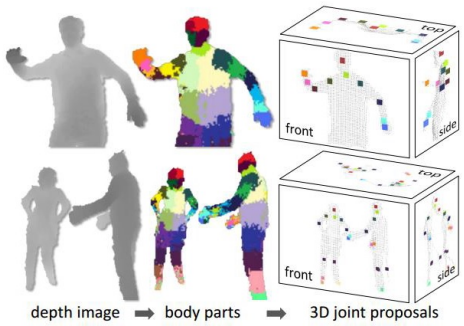

Figure 5: 3D Joint proposal from depth image (MacCormick, 2011).

walking direction of the person. In this work, it is assumed that the person will approximately walk in a straight line. Therefore the robot angle can be regulated by a much simpler controller. An angular velocity is applied when the difference between the heading angle and the torso angle of the person is greater than 0.1 radians.

2.2 Skeleton Tracking

Skeleton tracking is a feature provided by the Microsoft Kinect sensor. This depth camera consists of an infrared laser projector combined with a CMOS sensor, which captures 3-D real-time data. The sensing range of the depth sensor is adjustable, and the Kinect embedded software is capable of automatically calibrating the sensor based on the environment, accommodating for the presence of furniture or other obstacles. Due to the fact that the Kinect uses an infrared sensor, it can also operate in low lighting conditions. It produces a virtual skeleton which is detected by first composing a depth image, then labelling the body parts and finally estimating the positions of the joints in 3D. (MacCormick, 2011). Figure 5 gives a representation of the process.

The OpenNI Tracker package (Field, 2015) provides an interface for the skeleton detection software in the Robotic Operating System (ROS). It is provided by PrimeSense^{TM} and returns 3D positions of the following joints: head, torso, neck, shoulders, elbows, hands, hips, knees and feet.

2.3 Gait Parameters Extraction

The OpenNI tracker returns the raw joint coordinates of a subject's skeleton in the camera frame. Additional post-processing is required to obtain gait parameters from this data. Figure 6 illustrates the post-processing steps.

As explained in section 2.1 , the robot follows

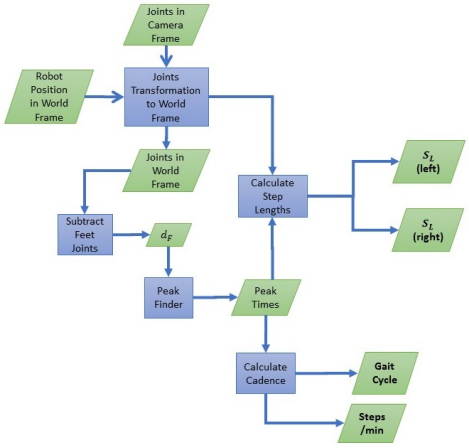

Figure 6: Calculating Gait Parameters.

the person during experiments. The joint coordinates are therefore expressed in a moving coordinate frame. The first step in obtaining the gait parameters is then to express the joint coordinates in a static frame. The camera is mounted at an angle relative to the floor. A rotation about the local y-axis can be used to align the joint coordinates with the floor (see Figure 3). Next, we transform the measurements from the moving frame to the fixed world frame. This transformation is achieved by using the robot pose (position and orientation). The internal encoders give the displacement of the robot between each timestep. By integrating these displacements, one can obtain a pose at each timestep relative to the initial pose. The joint positions in the aligned camera frame should thus also be rotated by the robot heading angle θ, and translated by the position of the robot. The joints in the world frame are thus obtained by:

$$\boldsymbol{P}_{world} = \boldsymbol{T}_{R,rob}\boldsymbol{T}_{T,rob}\boldsymbol{T}_{cam}\boldsymbol{P}_{cam}$$

$$\boldsymbol{T}_{cam} = \begin{bmatrix} \cos\beta & 0 & \sin\beta & 0 \\ 0 & 1 & 0 & 0 \\ -\sin\beta & 0 & \cos\beta & 0 \\ 0 & 0 & 0 & 1 \end{bmatrix}$$

$$\boldsymbol{T}_{T,rob} = \begin{bmatrix} 1 & 0 & 0 & x_{rob} \\ 0 & 1 & 0 & y_{rob} \\ 0 & 0 & 1 & z_{rob} \\ 0 & 0 & 0 & 1 \end{bmatrix} \quad (4)$$

$$\boldsymbol{T}_{R,rob} = \begin{bmatrix} \cos\theta & -\sin\theta & 0 & 0 \\ \sin\theta & \cos\theta & 0 & 0 \\ 0 & 0 & 1 & 0 \\ 0 & 0 & 0 & 1 \end{bmatrix}$$

Where $\boldsymbol{P}_{world}$ is the joint position in the world frame, $\boldsymbol{T}_{cam}$ is the camera rotation matrix, $\boldsymbol{T}_{T,rob}$ is the robot translation matrix, $\boldsymbol{T}_{R,rob}$ is the robot rotation matrix, $\boldsymbol{P}_{cam}$ is the joint position in the camera frame, β is the camera angle and θ is the robot heading angle (see

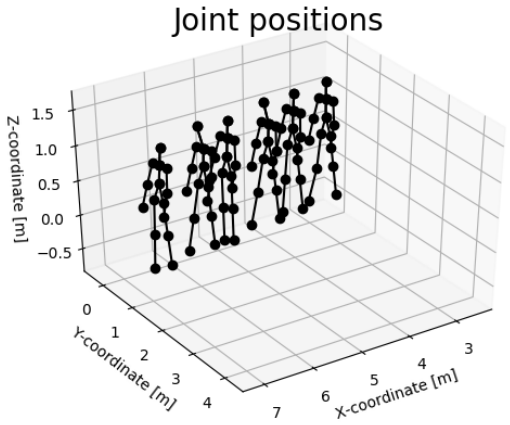

Figure 7: Movement of the joints in the world frame.

figure 3). Figure 7 shows the movement of the joints detected by the depth camera when converted to the world frame.

The most commonly used gait parameters are the gait cycle time, the cadence and the length of the steps. These can all be detected based on the feet positions. Figure 8 shows the movement of both feet during a typical gait cycle. At time t_1, the right foot is behind the left foot. The distance between the feet (d_F, see Figure 8) is maximum at this moment. Next, the person lifts their right foot and moves it next to the left foot at time t_2. The right foot is still in the air and d_F is now minimum. Finally, the person completes the step by moving the right foot in front of the left foot and placing it on the ground at t_3. The time difference between t_1 and t_3 is equal to the gait cycle time t_g. This can be converted to a number of steps per minute:

$$C_g = \frac{60}{t_g} \tag{5}$$

Where C_g is the cadence in steps per minute and t_g is the gait cycle time in seconds. The step length S_L is defined as the distance between the positions at the beginning and end of a step (positions at time t_1 and t_3 in Figure 8, respectively):

$$S_L = \sqrt{(x_b - x_e)^2 + (y_b - y_e)^2 + (z_b - z_e)^2} \tag{6}$$

Where x, y and z are used to represent the coordinates of the feet positions in the world frame and subscripts b and e are used to denote the start and end of a step, respectively.

It is clear that d_F will be an oscillating signal. Figure 9 shows an example of d_F as a function of time. Both the start and end of a step show up as a peak in this signal. Therefore we extract the timestamp and feet positions of every second peak. The time difference between two peaks is equal to the gait cycle time.

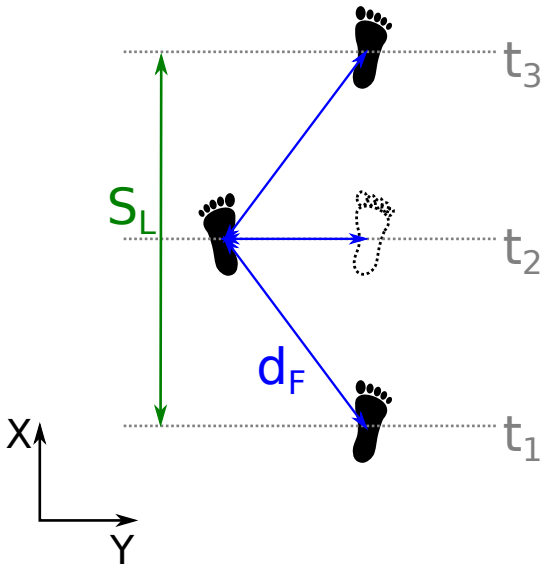

Figure 8: Movement of a persons feet during a step.

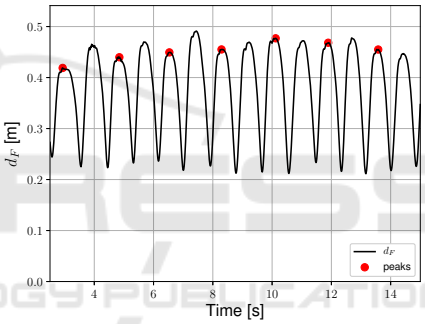

Figure 9: Distance between feet as a function of time.

The distance between every consecutive peak is equal to the step length.

This approach does not strictly require the rotation of the camera and robot frame to extract the gait parameters. Because this extraction is only based on distance vectors, it will still work even if the robot and camera angles are not compensated. While the movement along the individual coordinate axes in a rotated frame might be different, the total distance traveled is the same regardless of the orientation of the coordinate frame. This means that these angles do not have to be accurately measured, which reduces hardware requirements for our mobile platform. However, compensating the angles does enable better visualization. Translation to a fixed coordinate frame is required, and is prone to position measurement errors (see section 4.4).

2.4 Kalman Filter and RTS Smoother

The raw data that is returned by the OpenNI software is subject to noise. This can result in poor detection of the gait parameters. Better performance can be achieved by filtering the data before analysis. In order to achieve this we implemented a Kalman filter. The original formulation is a recursive algorithm that computes the state of a system at each time step. Additionally, the filter returns the uncertainty on each state estimate. The algorithm works according to a two step process. In the first step, a prediction of the next state is made based on a model of the system's dynamics. This step is also called the prediction step. The second step takes a state-dependent measurement as an input. This measurement is then compared to a model that predicts measurements based on the predicted state. The difference between the predicted and the real measurement is new information (also called the innovation). This is weighed with the predicted state in order to obtain the new state estimate. Mathematically, this is expressed as (Thrun et al., 2005):

$$\begin{aligned}
\hat{\boldsymbol{q}}_{n|n-1} &= \boldsymbol{F}_n \tilde{\boldsymbol{q}}_{n-1|n-1} + \boldsymbol{B}_n \boldsymbol{u}_n \\
\hat{\boldsymbol{P}}_{n|n-1} &= \boldsymbol{F}_n \tilde{\boldsymbol{P}}_{n-1|n-1} \boldsymbol{F}_n^T + \boldsymbol{Q}_n \\
\boldsymbol{\nu}_n &= \boldsymbol{z}_n - \boldsymbol{H}_n \hat{\boldsymbol{q}}_{n|n-1} \\
\boldsymbol{K}_n &= \hat{\boldsymbol{P}}_{n|n-1} \boldsymbol{H}_n^T \left(\boldsymbol{H}_n \hat{\boldsymbol{P}}_{n|n-1} \boldsymbol{H}_n^T + \boldsymbol{R}_n \right)^{-1} \\
\tilde{\boldsymbol{q}}_{n|n} &= \hat{\boldsymbol{q}}_{n|n-1} + \boldsymbol{K}_n \boldsymbol{\nu}_n \\
\tilde{\boldsymbol{P}}_{n|n} &= \left(I - \boldsymbol{K}_n \boldsymbol{H}_n \right) \hat{\boldsymbol{P}}_{n|n-1}
\end{aligned} \tag{7}$$

Where $\boldsymbol{q}$ is the state vector, $\boldsymbol{F}$ is the state transition matrix, $\boldsymbol{B}$ is the control input matrix, $\boldsymbol{u}$ is the control vector, $\boldsymbol{P}$ is the covariance matrix, $\boldsymbol{Q}$ is the process noise covariance matrix, $\boldsymbol{\nu}$ is the innovation, $\boldsymbol{z}$ is a measurement, $\boldsymbol{K}$ is the Kalman gain, $\boldsymbol{H}$ is the state observation matrix, $\boldsymbol{R}$ is the measurement noise covariance matrix and $\boldsymbol{I}$ is the identity matrix. Boldface symbols are used to represent matrix quantities (e.g., $\boldsymbol{F}$). A tilde symbol is used for estimated quantities (e.g., $\tilde{q}_n$), and a hat symbol is used for predicted quantities (e.g., $\hat{y}_n$). Subscripts n, and $n-1$ are used to denote timesteps.

In our case the goal is simply to smooth the data. Therefore: $\boldsymbol{F}_n = 1$, $\boldsymbol{H}_n = 1$, $\boldsymbol{B}_n = 0$ and $\boldsymbol{u}_n = 0$.

From (7) it can be seen that the state estimate at timestep n is only directly based on the estimate from timestep $n-1$ and the measurement at timestep n. This means that the estimate from timestep $n-1$ is in turn based on timestep $n-2$, and so on. Hence, the estimate at timestep n depends on all of the previous measurements, though to varying degrees. $n-1$ has the most influence, $n-2$ has the next most, and so on (Labbe, 2017). In our application, all the data has already been gathered. Therefore online state estimation is not necessary. The estimates can thus be improved by incorporating future data, which is the purpose of a smoothing filter. In this work, a fixed-interval Kalman smoother was implemented. This type of smoother uses all the measurements from a fixed observation interval in order to provide an optimal state-estimate (Sage and Melsa, 1971). We used the algorithm proposed in (Rauch et al., 1965). This is an efficient implementation of a fixed-interval smoother that is easy to implement. It makes two passes over the data. In the first or forward pass, the algorithm works like a regular Kalman filter. The state estimates and corresponding covariance matrices at each step are saved. In the second or backward pass, the Rauch, Tung and Striebel smoother (RTS smoother) runs over the data in the opposite direction according to the following equations:

$$\begin{aligned}
\boldsymbol{C}_n &= \boldsymbol{P}_{n|n} \boldsymbol{F}_{n+1}^T \boldsymbol{P}_{n+1|n}^{-1} \\
\hat{\boldsymbol{q}}_{n|k} &= \hat{\boldsymbol{q}}_{n|n} + \boldsymbol{C}_n \left(\hat{\boldsymbol{q}}_{n+1|k} - \hat{\boldsymbol{q}}_{n+1|n} \right) \\
\boldsymbol{P}_{n|k} &= \boldsymbol{P}_{n|n} + \boldsymbol{C}_n \left(\boldsymbol{P}_{n+1|k} - \boldsymbol{P}_{n+1|n} \right) \boldsymbol{C}_n^T
\end{aligned} \tag{8}$$

It is clear that during the second pass, knowledge of the future is incorporated in the state estimate. When the first measurement is reached, the filtered output includes all information in a maximally optimal form (Labbe, 2017).

3 EXPERIMENTAL SETUP

3.1 Mobile Platform

A ROS-based mobile robot (TurtleBot) was used for the experiments. ROS allows researchers to easily modify and extend the software according to their desired application. Built-in wheel encoders enable the estimation of the robot's position relative to the starting location. The TurtleBot is able to acquire visual information using the Microsoft Kinect Sensor.

The mobile platform also has a laptop on top which is running the subject tracking and following algorithms. The robot was covered with a custom made dress to obtain a more appealing look to the subjects. Furthermore, the laptop display was used as an interaction device through an animated face. The face animation changes according to the robot state. A happy face animation provides feedback of successful subject detection and tracking, while a sad face is displayed if there is no subject or in case the subject is

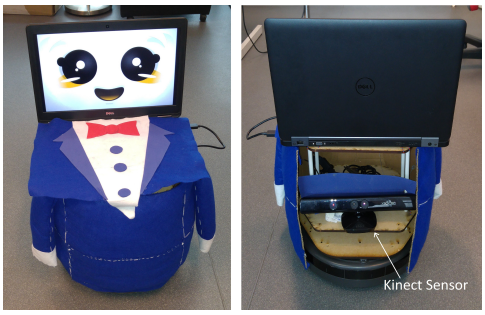

Figure 10: (left) Front of the mobile platform (right) Back of the mobile platform.

lost. Sound feedback is also used during tracker initialization. Figure 10 shows the front and back of the mobile platform.

3.2 Validation

In order to compare and validate the joint movements tracked by the mobile platform, experiments were performed in the MALL (Movements posture & Analysis Laboratory Leuven) of Faculty of Kinesiology and Rehabilitation Sciences, Leuven. A motion capture system based on 10 VICON cameras enables the measurement of 3-D joint motion. This system allows analysis of human movement by placing passive markers on the subject to measure the orientation and rotation of body segments. By combining the information of adjacent segments, joint angle trajectories can be calculated. The length of the testing area is limited to six meters.

3.3 Experiments in the Care Home

Besides validation experiments, informal tests were also conducted in the care facility Edouard Remy in Leuven. These tests were conducted within the ethical and social guidelines of the carehome, and with consent of both the staff and the residents. Additionally, a staff member was always present during testing. The residents are mainly seniors aged 65 or above. Some still have the ability to take care of themselves but need help with cooking or cleaning, while others have a mental or physical illness that makes them require regular assistance. The goal of these experiments was to evaluate the behavior in a more crowded environment. Additionally, we wanted to get the response of residents to our system.

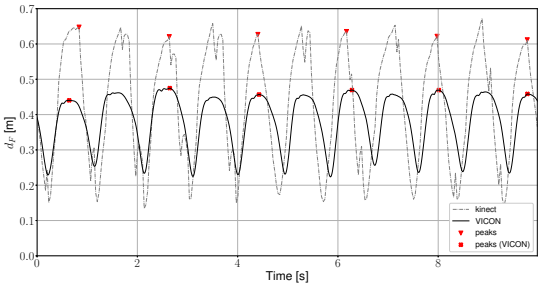

Figure 11: Feet distance based on raw measurements (camera angle = 25°).

4 EXPERIMENTAL RESULTS

4.1 Raw Gait Data

A total of 9 experiments were conducted, 4 with a camera angle of 25° and 5 with a camera angle of 30°. For each experiment, between 5 and 7 steps could be measured by the VICON camera before the test subject moved out of the field of view. One dataset with a camera angle of 30° was chosen as a calibration dataset to determine the filter parameters. This dataset was therefore not included in the error calculations. One of the co-authors (a healthy adult male) was used as a test subject for all experiments. The procedure outlined in section 2.3 was followed to obtain the gait parameters from the joint data. The same procedure was used to obtain gait parameters from the VICON data. Figure 11 shows the distance between the feet as measured by the Kinect and VICON systems. From this figure it can be seen that the Kinect systematically overestimates the distance between the feet. This is in part likely due to the fact that the VICON and the Kinect detect different markers. If the VICON detects a marker at the inside of a foot, and the Kinect detects a marker at the middle or outside of a foot, then this will give an offset difference. The difference observed in Figure 11 is quite large though, indicating that there are other sources of error as well. Most likely the Kinect suffers from detection errors.

The Kinect measurements are assessed in terms of absolute error and relative error with respect to the VICON measurements which serve as the ground truth. Table 1 shows the average error ($\bar{e}$) and standard deviation (σ_e) for both camera angles. From the results, it can be observed that the proposed monitoring setup is able to accurately detect the times at which a step occurs. At a camera angle of 25°, the average error is less than 1 step per minute (approximately 2%). At a camera angle of 30°, the error is slightly larger at approximately 2 steps per minute or 5%. The standard deviation in this case is quite large relative to the

Table 1: Error of raw Kinect measurements. Top: absolute error with respect to VICON measurements. Bottom: relative error with respect to VICON measurements.

	$\bar{e}$ (25°)	σ_e (25°)	$\bar{e}$ (30°)	σ_e (30°)
C_g [SPM]	0.68	0.61	-1.73	2.13
t_g [s]	-0.03	0.03	0.10	0.13
S_L left [m]	0.24	0.05	0.13	0.05
S_L right [m]	0.22	0.05	0.12	0.05
C_g [%]	1.91	1.66	-5.15	6.37
t_g [%]	-1.86	1.59	5.79	7.13
S_L left [%]	60.86	14.81	30.92	14.17
S_L right [%]	51.98	11.43	29.29	14.07

mean, indicating a wide spread of the data and thus an imprecise measurement. Calculation of step length proves to be much more challenging. The proposed approach consistently overestimates the step length. The camera angle also plays a more important role compared to step time detection. For an angle of 25°, the average error on a single step is a little over 20 cm (50% - 60%), while for 30°, the average error is a slightly more than 12 cm (approximately 30%). Although changing the camera angle results in significant improvement, the error on the step length is too large and hence not directly suitable for clinical applications.

4.2 Kalman Filter

It can be observed from Figure 11 that the raw data from the Kinect has a significant degree of noise. The sudden changes and noisy peaks result in poor gait parameters extraction compared to the VICON data. Additionally, the feet distance is much larger than for the VICON measurements, which causes a consistent overestimation of the step length. In order to improve performance, we implemented a Kalman filter. In its standard form, this algorithm only relies on past data. So even though we use it to filter the data in postprocessing, the Kalman filter could also be used to estimate the gait parameters during the experiment. The filtering is carried out on the raw joint coordinates in the world frame (before the calculation of d_F). The process and measurements variances (Q and R, respectively) are therefore expressed in meters. One dataset with a camera angle of 30° was chosen as a calibration dataset. Through trial and error, we determined that a Q of 0.0003m and a R of 0.01m provide satisfactory results on this calibration dataset. The same parameters were then applied to the other datasets. Our filter is thus only calibrated on a single dataset. Figure 12 shows d_F after applying a Kalman filter to the raw data. It can be seen that the filter is

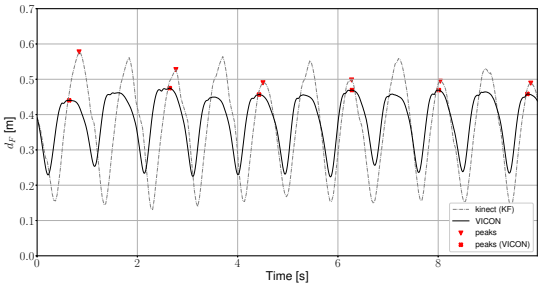

Figure 12: Feet distance based on Kinect measurements after Kalman filtering (camera angle = 25°).

able to smooth most of the noisy peaks that can be observed in Figure 11. Additionally, the measurements now more closely resemble the VICON data. The Kalman filter does introduce a small delay. However, it is not necessary for the validation that the Kinect and the VICON measurements are exactly time synchronized, as long as the same steps are measured. Figure 11 is only for visualization purposes and is not exactly time synchronized.

Table 2 summarizes the absolute and relative error after filtering, respectively. It can be observed that the use of a Kalman filter drastically improves gait parameter extraction on most fronts. For a camera angle of 25°, the average error on the cadence is only 0.3 steps per minute. The standard deviation did however increase to about 1 step per minute. For a camera angle of 30°, there is almost no error on step time detection, and the standard deviation is only 30 milliseconds. The step length is still consistently overestimated, however. On average, the estimate based on the filtered measurements deviates from the VICON measurements by approximately 10 cm (20% to 30%). Again, one can observe that using a camera angle of 30° improves results further. There is almost no difference in cadence compared to the VICON measurements. The error on the step length is in this case approximately 5cm (10% to 12%). Though the spread of these results is larger.

4.3 RTS Smoother

A final improvement to the detection process can be made by smoothing the data after the experiment has been completed. In contrast to the Kalman filter, this approach cannot be used for online estimation of the gait parameters. However, this is not necessary in all applications. Therefore we also present the results of this method. Figure 13 shows d_F after processing the kinect data with an RTS smoother. The same values for Q and R as in section 4.2 were used. Improvement is more gradual then when we added the Kalman filter to the raw data. One can observe, however, that

Table 2: Error of measurements after Kalman filtering. Top: absolute error with respect to VICON measurements. Bottom: relative error with respect to VICON measurements.

	$\bar{e}$ (25°)	σ_e (25°)	$\bar{e}$ (30°)	σ_e (30°)
C_g [SPM]	-0.30	1.27	0.06	0.59
t_g [s]	0.01	0.06	0.00	0.03
S_L left [m]	0.12	0.02	0.05	0.06
S_L right [m]	0.09	0.04	0.04	0.02
C_g [%]	0.31	1.82	-1.11	3.47
t_g [%]	0.87	3.66	-0.16	1.77
S_L left [%]	31.16	8.44	12.05	14.07
S_L right [%]	20.34	10.17	10.33	6.15

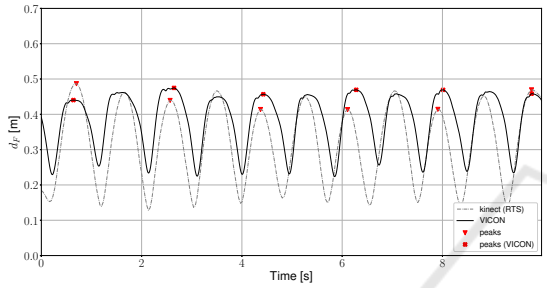

Figure 13: Feet distance based on Kinect measurements after RTS smoother (camera angle = 25°).

Table 3: Error of Kinect measurements after RTS smoother. Top: absolute error with respect to VICON measurements. Bottom: relative error with respect to VICON measurements.

	$\bar{e}$ (25°)	σ_e (25°)	$\bar{e}$ (30°)	σ_e (30°)
C_g [SPM]	0.26	0.35	-0.10	0.57
t_g [s]	-0.01	0.02	0.01	0.03
S_L left [m]	0.03	0.01	-0.04	0.05
S_L right [m]	0.01	0.02	0.02	0.03
C_g [%]	0.72	0.98	-0.30	1.70
t_g [%]	-0.71	0.97	0.32	1.72
S_L left [%]	8.60	2.94	-8.26	11.36
S_L right [%]	1.25	5.42	3.93	6.15

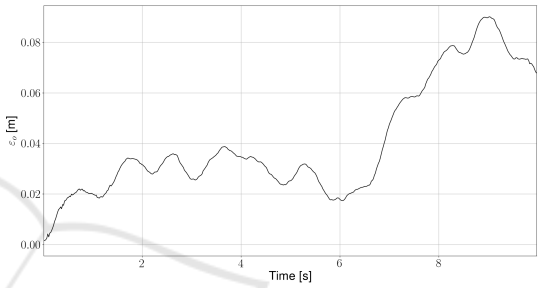

Figure 14: Drift of the robot frame.

the RTS-smoother flattens the residual deformations that can be seen in Figure 12. Additionally, the oscillations are now of the same order of magnitude as the VICON measurements.

Table 3 gives the absolute and relative error with respect to the VICON data after applying the RTS smoother. No large improvements can be observed for cadence detection apart from the lower standard deviation of the cadence for a camera angle of 25°. However, these results were already satisfactory. Improvements have been made in regards to step length detection. The error on the detected step length is now between 2 cm and 4 cm. This translates to a relative error between 4% and 8%. For the first time, little difference can be observed between a camera angle of 25° and a camera angle of 30°. This illustrates the increased robustness of the RTS smoother.

4.4 Robot Position Estimates

The robot pose estimates are used to transform the joint coordinates to a static world frame. These pose estimates are achieved by integrating the displacements provided by the internal encoders. Because each measurement has a slight error, this leads to a drift in position over time. As a result, the world frame will not be fixed. This has an influence on the gait parameter extraction. Because the orientation of the VICON coordinate system is not known, this can only be verified based on the distance to the origin:

$$r_o = \sqrt{(x_1 - x_0)^2 + (y_1 - y_0)^2 + (z_1 - z_0)^2} \quad (9)$$

Where r_o is the distance to the origin, and subscripts 1 and 0 are used to denote the position at the start and end of the experiment, respectively. Figure 14 shows the difference between the distance to the origin of the robot frame as measured by both the VICON and the encoders (that is, $\varepsilon_o = r_{o,VICON} - r_{o,robot}$). From this figure it can be seen that the error occasionally decreases, as negative errors get integrated for a short period. Overall though, the positioning error increases. At the end of the 5 m trajectory, the error is approximately 7 cm. We repeated this process for other datasets. On average, the error for each dataset is 10 cm. However, it is not the total drift that determines the accuracy. Because we are using displacements, only the drift between steps will have an influence on the gait parameter extraction. This drift will be much smaller. Therefore we also calculated the drift between steps for all datasets, which is equal to 1cm on average.

4.5 Experiments in the Care Home

In the first phase, we conducted tests without the dress and face. Residents were much more disapproving of the robot in this form, which prompted us to overhaul its appearance. This lead to a much more positive response. Residents were interested about our robot and were much more willing to participate in our experiments.

Both the person detection and joint tracking software were able to perform their tasks satisfactory even in the presence of multiple persons. The person that was most visible in the image during initialization (i.e. was the biggest detected blob) was chosen as the subject to track. After which, the tracking algorithms were able to distinguish between different persons in the image. However, in areas with insufficient lighting, the webcam was not always able to detect the presence of a person.

Even though the residents generally have slower walking speed than healthy adults, they still reported that the speed of the robot was too slow for them.

Finally, tracking has to be initialized by having the subject perform a psi-pose, which could be a problem for patients that have limited mobility. However, all subjects in the care facility were able to initialize the tracking. A patient who had previously sustained a stroke had some difficulty, but was also able to perform the psi-pose and initialize the tracking on his own.

5 DISCUSSION

The cost of the proposed system is minimal compared to other optical gait analysis systems (Mihradi et al., 2011a). Other cost-effective methods for gait analysis, such as wearable devices (Yang and Hsu, 2010; O'Donovan et al., 2009) or pressure insoles (Crea et al., 2014), are usually limited to measuring very few gait parameters, thus requiring an array of sensors. Our method can be extended to measure other parameters, such as lower limb angular velocities and core posture, at the cost of increased computational complexity. By using the distance between the feet instead of the motion along a single coordinate axis (for example the z-axis of the foot), we eliminate the need for an accurate determination of the robot or camera angle. By mounting the depth camera on a mobile platform, we are not limited to the field of view of the camera, as is the case with static cameras. This allows for much longer continuous measurements. Important gait indicators can be extracted unobtrusively while the subject performs daily activities as the robot actively follows and tracks the skeletal joint movements unlike static systems (Geerse et al., 2015; Fern'ndez-Baena et al., 2012). The raw Kinect data is subject to a relatively high degree of noise. This is partly due to fluctuations in the detected feet positions. Another contributing factor is the vibrations of the robot platform while it is driving. Loose clothing can also cause errors in detecting the joint positions. Moreover, the foot displacements are consistently overestimated. Therefore the raw Kinect data is not directly suitable for gait detection and filtering is thus required. This can be done while the experiment is taking place with the Kalman filter, though better performance can be reached by using an RTS-smoother after the experiment has finished. Estimating the gait parameters during an experiment can be useful for rehabilitation. Patients could get immediate feedback that tells them whether they are putting in too much or too little effort.

The ability to extract gait quality parameters such as step lengths, cadence and gait cycle with a dynamic platform could benefit a variety of populations requiring rehabilitation and assistive care. Providing that an overall view of the patients gait quality is needed, results in this paper showed that measuring these parameters with our mobile robot has similar performance to what was reported in (Baldewijns et al., 2014) and (Geerse et al., 2015). The results were validated with VICON motion analysis system. We showed that orientation of the camera influences results significantly when using the raw data or the Kalman filter. At 30°, the Kinect camera sees a bigger section of the person. This allows it to more accurately estimate the positions of the feet. As a result, the gait parameters can be estimated more accurately. The RTS smoother is less dependent on the camera angle.

Future improvements will result in a much more complete mobile biomonitoring solution. One of the current limitations is the maximum speed of the robot of 0.2 m/s. This necessitates a slower than normal walking speed during the experiments. Thus, a robot platform with higher maximum speed would be a necessary improvement. Moreover, wheel encoders do not provide a very accurate position estimation over long distances. The integration of measurement errors will cause a drift in position over time, thus affecting the gait measurements. Relying only on encoder measurements does not provide a global position or a relative position of obstacles with respect to the robot. Hence, it is not possible to avoid unexpected obstacles or let the robot navigate autonomously when it is not monitoring people. Thus, extending the sensing ability of the robot with a laser scanner will allow

the robot to autonomously navigate, avoid obstacles and localize itself more accurately in a known map. Alternatively, data from the Kinect could be used for localization. As mentioned in section 2, this requires modifications to the OpenNI source code. However, this would allow the use of a single sensor for both localization, joint and person detection, which significantly lowers hardware costs. The controller that was used is quite a simple implementation. It keeps a relatively constant distance between the person and the robot. Future experiments could determine the optimal following distance and angle, and optimally control the robot trajectory accordingly. Additionally, a single state-feedback controller could be used to control all variables of interest. Tracking has to be initialized by letting the subject perform a psi-pose, which impairs autonomous operation of the system. This is an important drawback over other systems which do not require this initialization.

Finally, the Kalman filter variances were determined through trial and error with a single calibration dataset. Therefore a reference system is still needed to calibrate the system once with a single dataset. Afterwards, the robot can be used without the external reference. By automatically calculating these parameters, the robustness of the proposed approach could be increased. This could be achieved by, for example, using the expectation-maximization algorithm (Khan and Dutt, 2007).

6 CONCLUSION

In this paper, we proposed a marker less gait parameter extraction method with simultaneous tracking of the subject by using a Kinect sensor mounted on a mobile robot. This overcomes the limitations of a fixed test space for gait analysis. Compared to the existing gait analysis systems, this proof of concept work proposes a cost effective approach which can be used in different clinical applications. The acquired skeletal joint data is further processed to extract important gait parameters such as gait cycle time, step length and cadence, which are related to different diseases and neurological disorders. We propose methods for online and offline gait parameter extraction and compare the results for both methods. The state feedback controller allows continuous following of the subject while measuring joint positions. We succeeded in visualizing the gait performance and validated the extracted information with a VICON motion capture system. We confirmed the usefulness of our proposed method by comparing the results with previous studies. The results presented in this research are in good agreement with previous studies despite being dynamic. However, a calibration with a more accurate monitoring system is required. Future work will focus on developing a more suitable robot platform, that has a higher maximum speed and more interaction capabilities such as a touchscreen. Additionally, a more sophisticated controller would enable better following behavior in more complex environments. Finally, tracking has to be initialized manually by performing a psi pose. Automatic starting and stopping of measurements would allow fully autonomous operation of the robot.

ACKNOWLEDGEMENTS

The authors would like to thank MALL (Movements posture & Analysis Laboratory Leuven) of the Faculty of Kinesiology and Rehabilitation Sciences Leuven for providing the motion analysis facilty equipped with a VICON motion capture system in order to validate the proposed platform. Special thanks goes out to the care facility Edouard Remy in Leuven, for the opportunity to perform experiments and for their input. Robin Amsters is an SB fellow of the Research Foundation Flanders (FWO) under grant agreement 1S57718N.

REFERENCES

Baldewijns, G., Verheyden, G., Vanrumste, B., and Croonenborghs, T. (2014). Validation of the kinect for gait analysis using the gaitrite walkway. In *Engineering in Medicine and Biology Society (EMBC), 2014 36th Annual International Conference of the IEEE*, pages 5920–5923. IEEE.

Crea, S., Donati, M., Rossi, S. M. M. D., Oddo, C. M., and Vitiello, N. (2014). A Wireless Flexible Sensorized Insole for Gait Analysis. *Sensors (Basel, Switzerland)*, 14(1):1073–1093.

European Commission (2014). The 2015 ageing report: Underlying assumptions and projection methodologies.

Fern'ndez-Baena, A., Susn, A., and Lligadas, X. (2012). Biomechanical validation of upper-body and lower-body joint movements of kinect motion capture data for rehabilitation treatments. In *2012 Fourth International Conference on Intelligent Networking and Collaborative Systems*, pages 656–661.

Field, T. (2015). openni_tracker-ros wiki.

Geerse, D. J., Coolen, B. H., and Roerdink, M. (2015). Kinematic validation of a multi-kinect v2 instrumented 10-meter walkway for quantitative gait assessments. *PLOS ONE*, 10(10):1–15.

Goffredo, M., Bouchrika, I., Carter, J. N., and Nixon, M. S. (2010). Performance analysis for automated gait ex-

traction and recognition in multi-camera surveillance. *Multimedia Tools and Applications*, 50(1):75–94.

Hausdorff, J. M., Lertratanakul, A., Cudkowicz, M. E., Peterson, A. L., Kaliton, D., and Goldberger, A. L. (2000). Dynamic markers of altered gait rhythm in amyotrophic lateral sclerosis. *Journal of applied physiology*, 88(6):2045–2053.

Hausdorff, J. M., Rios, D. A., and Edelberg, H. K. (2001). Gait variability and fall risk in community-living older adults: A 1-year prospective study. *Archives of Physical Medicine and Rehabilitation*, 82(8):1050 – 1056.

Hodgins, D. (2008). The importance of measuring human gait. *Medical Device Technology*, 19(5):42–44.

Hoff, J., Wagemans, E., Van Hilten, J., et al. (2001). Accelerometric assessment of levodopa-induced dyskinesias in parkinson's disease. *Movement disorders*, 16(1):58–61.

Kavanagh, J. J. and Menz, H. B. (2008). Accelerometry: a technique for quantifying movement patterns during walking. *Gait & posture*, 28(1):1–15.

Keijsers, N. L., Horstink, M. W., and Gielen, S. C. (2003). Movement parameters that distinguish between voluntary movements and levodopa-induced dyskinesia in parkinsons disease. *Human movement science*, 22(1):67–89.

Keijsers, N. L., Horstink, M. W., and Gielen, S. C. (2006). Ambulatory motor assessment in parkinson's disease. *Movement Disorders*, 21(1):34–44.

Khan, M. E. and Dutt, D. N. (2007). An Expectation-Maximization Algorithm Based Kalman Smoother Approach for Event-Related. *Transaction of biomedical engineering*, 54(7):1191–1198.

Labbe, R. R. (2017). *Kalman and Bayesian Filters in Python*.

Leu, A., Ristić-Durrant, D., and Gräser, A. (2011). A robust markerless vision-based human gait analysis system. In *Applied Computational Intelligence and Informatics (SACI), 2011 6th IEEE International Symposium on*, pages 415–420. IEEE.

Liu, T. and Liu, J. (2014). Mobile robot aided silhouette imaging and robust body pose recognition for elderly-fall detection. *International Journal of Advanced Robotic Systems*, 11(3):42.

Luinge, H. J. and Veltink, P. H. (2005). Measuring orientation of human body segments using miniature gyroscopes and accelerometers. *Medical and Biological Engineering and computing*, 43(2):273–282.

MacCormick, J. (2011). How does the kinect work. *Presentert ved Dickinson College*, 6.

Mihradi, S., Dirgantara, T., Mahyuddin, A. I., et al. (2011a). Development of an optical motion-capture system for 3d gait analysis. In *Instrumentation, Communications, Information Technology, and Biomedical Engineering (ICICI-BME), 2011 2nd International Conference on*, pages 391–394. IEEE.

Mihradi, S., Dirgantara, T., Mahyuddin, A. I., et al. (2011b). Development of an optical motion-capture system for 3d gait analysis. In *Instrumentation, Communications, Information Technology, and Biomedical Engineering (ICICI-BME), 2011 2nd International Conference on*, pages 391–394. IEEE.

O'Donovan, K. J., Greene, B. R., McGrath, D., O'Neill, R., Burns, A., and Caulfield, B. (2009). Shimmer: A new tool for temporal gait analysis. In *Engineering in Medicine and Biology Society, 2009. EMBC 2009. Annual International Conference of the IEEE*, pages 3826–3829. IEEE.

Peel, N. M., Kuys, S. S., and Klein, K. (2013). Gait speed as a measure in geriatric assessment in clinical settings: a systematic review. *The Journals of Gerontology: Series A*, 68(1):39–46.

Rauch, H. E., Striebel, C. T., and Tung, F. (1965). Maximum likelihood estimates of linear dynamic systems. *AIAA Journal*, 3(8):1445–1450.

Sage, A. and Melsa, J. (1971). Estimation theory with applications to communications and control. Technical report, Southern methodist univ Dallas tex information and control sciences center.

Shotton, J., Sharp, T., Kipman, A., Fitzgibbon, A., Finocchio, M., Blake, A., Cook, M., and Moore, R. (2013). Real-time human pose recognition in parts from single depth images. *Communications of the ACM*, 56(1):116–124.

Sontag, E. D. (2013). *Mathematical control theory: deterministic finite dimensional systems*, volume 6. Springer Science & Business Media.

Stone, E. E. and Skubic, M. (2011a). Evaluation of an inexpensive depth camera for passive in-home fall risk assessment. In *Pervasive Computing Technologies for Healthcare (PervasiveHealth), 2011 5th International Conference on*, pages 71–77. Ieee.

Stone, E. E. and Skubic, M. (2011b). Passive in-home measurement of stride-to-stride gait variability comparing vision and kinect sensing. In *Engineering in Medicine and Biology Society, EMBC, 2011 Annual International Conference of the IEEE*, pages 6491–6494. IEEE.

Thrun, S., Burgard, W., and Fox, D. (2005). *Probabilistic robotics*. MIT press.

Van Den Broeck, B., Vuegen, L., Van Hamme, H., Moonen, M., Karsmakers, P., and Vanrumste, B. (2013). Footstep localization based on in-home microphone-array signals. *Assistive Technology: From Research to Practice: AAATE 2013*, 33:90.

Van Kan, G. A., Rolland, Y., Andrieu, S., Bauer, J., Beauchet, O., Bonnefoy, M., Cesari, M., Donini, L., Gillette-Guyonnet, S., Inzitari, M., et al. (2009). Gait speed at usual pace as a predictor of adverse outcomes in community-dwelling older people an international academy on nutrition and aging (iana) task force. *The journal of nutrition, health & aging*, 13(10):881–889.

Viccaro, L. J., Perera, S., and Studenski, S. A. (2011). Is timed up and go better than gait speed in predicting health, function, and falls in older adults? *Journal of the American Geriatrics Society*, 59(5):887–892.

Viola, P. and Jones, M. (2001). Rapid object detection using a boosted cascade of simple features. In *Computer Vision and Pattern Recognition, 2001. CVPR 2001. Proceedings of the 2001 IEEE Computer Society Conference on*, volume 1, pages I–I. IEEE.

Wahid, N., Rahmat, M. F., and Jusoff, K. (2010). Comparative assesment using lqr and fuzzy logic controller for

a pitch control system. *European Journal of Scientific Research*, 42(2):184–194.

Wren, T. A., Gorton, G. E., Ounpuu, S., and Tucker, C. A. (2011). Efficacy of clinical gait analysis: A systematic review. *Gait & posture*, 34(2):149–153.

Yang, C.-C. and Hsu, Y.-L. (2010). A review of accelerometry-based wearable motion detectors for physical activity monitoring. *Sensors*, 10(8):7772–7788.

Yoo, J.-H. and Nixon, M. S. (2011). Automated marker-less analysis of human gait motion for recognition and classification. *Etri Journal*, 33(2):259–266.